Synthesis, biological evaluation and molecular docking studies of flavone and isoflavone derivatives as a novel class of KSP (kinesin spindle protein) inhibitors

ARTICLE *in* EUROPEAN JOURNAL OF MEDICINAL CHEMISTRY · OCTOBER 2013

Impact Factor: 3.45 · DOI: 10.1016/j.ejmech.2013.09.042 · Source: PubMed

8 AUTHORS, INCLUDING:

Yong-Hua Yang
Nanjing University
40 PUBLICATIONS **687** CITATIONS
SEE PROFILE

Xiao-Ming Wang
Nanjing University ,State Key Laboratory of…
27 PUBLICATIONS **155** CITATIONS
SEE PROFILE

European Journal of Medicinal Chemistry 70 (2013) 427–433

Contents lists available at ScienceDirect

European Journal of Medicinal Chemistry

journal homepage: http://www.elsevier.com/locate/ejmech

Original article

Synthesis, biological evaluation and molecular docking studies of flavone and isoflavone derivatives as a novel class of KSP (kinesin spindle protein) inhibitors

Jing-Jun Dong [a,1], Qing-Shan Li [a,b,1], Zhi-Peng Liu [a], Shu-Fu Wang [a], Meng-Yue Zhao [a], Yong-Hua Yang [a,*], Xiao-Ming Wang [a,*], Hai-Liang Zhu [a,*]

[a] State Key Laboratory of Pharmaceutical Biotechnology, Nanjing University, Nanjing 210093, PR China
[b] School of Medical Engineering, Hefei University of Technology, Hefei 230009, PR China

ARTICLE INFO

Article history:
Received 4 August 2013
Received in revised form
18 September 2013
Accepted 20 September 2013
Available online 2 October 2013

Keywords:
KSP
Flavone
Isoflavone
Antimitotic
Kinesin inhibitor
Monoastral spindles

ABSTRACT

The kinesin spindle protein (KSP) is involved in the formation of bipolar mitotic spindle during cell division and it becomes a new target to overcome the neurotoxicity of MTs inhibitors. A series of flavone and isoflavone derivatives (**1a**–**7c**) have been designed, synthesized and evaluated as potential KSP inhibitors. Among them, **2c** displayed the most potent inhibitory activity *in vitro*, which inhibited the growth of MCF-7 and Hela cell lines with IC_{50} values of 4.8 and 4.3 μM, respectively, and also exhibited significant KSP inhibitory activity (IC_{50} = 0.023 μM). The new compounds can induce irregular monoastral spindles, the characteristic phenotype for KSP inhibiting agents. Docking simulation was further performed to determine the probable binding model.

1. Introduction

The studies of mitotic inhibitors have been carried out and some antimitotic agents, such as colchicines, taxanes, vinblastine and some synthetic agents, show anticancer activity by binding to the β-tubulin protein (a component of the microtubule) [1]. However, because microtubules are also important in other nonproliferating cells and required for such processes as cell signaling and vesicular transport, the inhibition of microtubules leads to severe neurotoxicity and peripheral neuropathy [2,3]. Moreover, these compounds encounter the acquired resistance through a variety of mechanisms after the long-term use. Therefore, more specific and potential agents are needed to investigate and overcome the observed neuropathic side effects and drug resistance.

The kinesin spindle protein (KSP, also known as HsEg5) has recently gained significant attention as a novel biological target for anticancer therapy. KSP, a member of the kinesin-5 family, plays a critical role in centrosome separation and the formation and maintenance of the bipolar spindle [4]. Inhibition of the KSP in proliferating tumor cells leads to the failure of the centrosome separation and consequently irregular formation of a monopolar spindle, ultimately, resulting in cell death [5]. Since KSP is absent from adult central/peripheral nervous system neurons, which are postmitotic, KSP inhibitors are not expected to cause the disruption of the neuronal tubulin network [6,7]. And because of the overexpression of KSP in proliferating human solid tumors, such as breast, lung, ovarian, colon and bladder cancers, and leukemias [8–10], the inhibitors might work as selective agents for the treatment of malignant tumors.

Accordingly, significant efforts have been made in developing KSP inhibitors over the past decade since monastrol (Fig. 1), the first identification of the KSP inhibitor that can cause mitotic arrest with monopolar spindles, was reported by Mayer et al. [6] A number of KSP inhibitors have been reported, namely MK-0731 [11], ARRY-520 [12], ispinesib (SB715992) (Fig. 1), and several other small molecules [13–15]. These reported inhibitors are suggested to bind to an induced-fit pocket generating by helices α2 and α3 and loop L5 of the KSP [7,16]. Of these compounds,

* Corresponding authors. Tel./fax: +86 25 83592672.
E-mail address: zhuhl@nju.edu.cn (H.-L. Zhu).
[1] Both authors contributed equally to this work.

0223-5234/$ – see front matter © 2013 Elsevier Masson SAS. All rights reserved.
http://dx.doi.org/10.1016/j.ejmech.2013.09.042

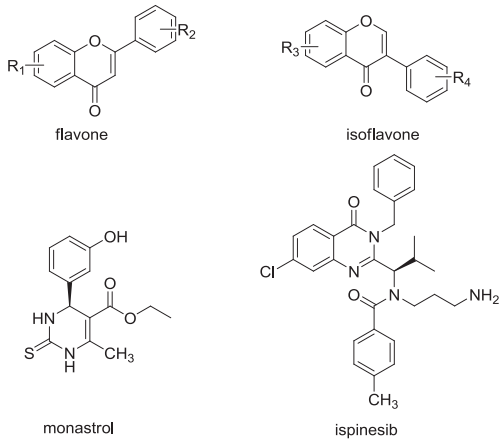

Fig. 1. Chemical structures of flavone, isoflavone and KSP inhibitors.

ispinesib was the first KSP inhibitor in phase 2 clinical trials [17]. Encouraged by these findings, we have tried our best to discover further KSP inhibitors.

Flavones or isoflavones (Fig. 1), such as genistein, have been reported to have many biological activities including anti-proliferative, [18] anti-inflammatory [19], anti-estrogenic [20] and anti-oxidant effects [21]. Many researchers also found that some of them could inhibit the activation of nuclear transcription factor κB (NF-κB), a sequence-specific transcription factor that can maintain the balance between cell survival and programmed cell death [22]. However, few reports have been dedicated for studying its KSP inhibitory activity. Many drugs containing nitrobenzotrifluoride possess anticancer activity because of their strong electron attracting ability. Upon interaction with the tumor cells, the electrophilic groups (CF_3, NO_2) of these drugs get tightly bind to nucleophiles present in and around the cells. Additionally, by introduction of the electron-withdrawing group CF_3, the lipophilicity of the compounds might become better for its penetration through the cell membrane [23]. Taking these factors into consideration, we tried to combine these advantages together to find new KSP inhibitors with enhanced activity.

Herein, we are reporting in the present work the design, synthesis and biological evaluation of new compounds, which contain flavone or isoflavone and nitrobenzotrifluoride simultaneously, as a novel class of KSP inhibitors. Biological evaluation indicated that some of the synthesized compounds were potent KSP inhibitors preliminarily. Mitotic phenotype helped us to seek their role in inducing cell death further, with the findings that these compounds could induce the monoastral spindles. Docking simulations were also performed using the X-ray crystallographic structure of the KSP in complex with an inhibitor to explore the binding modes of these compounds.

2. Results and discussion

2.1. Chemistry

The synthesis of flavone and isoflavone derivatives followed the general reaction pathway outlined in Scheme 1. Compounds **1a**–**7c** were synthesized by coupling substituted dinitro-compounds with equimolar (series A) or double mole quantities (series B) of flavones or isoflavones in DMF using t-BuOK as catalyst. All the compounds **1a**–**7c** were reported for the first time. All of the synthetic compounds gave satisfactory analytical and spectroscopic data. ^{1}H NMR and ESI-MS spectra were consistent with the assigned structures.

2.2. Crystal structure of compound *4a* and *4c*

Among these compounds, the crystal structure of compound **4a** and **4c** was determined by X-ray diffraction analysis. The crystallographic data for the structural analysis have been deposited with the Cambridge Crystallographic Data Centre Nos. 960224 for **4a** and Nos. 960225 for **4c**. The perspective views of **4a** and **4c** with the atomic labeling system were presented in Fig. 2.

2.3. Bioassay

2.3.1. Antiproliferative activity

To test the anticancer activities of the synthesized compounds, we evaluated antiproliferative activities of compounds **1a**–**7c** against MCF-7 (human breast cancer cell lines) and Hela cells. The results were summarized in Table 1. To our delight, a number of flavone and isoflavone derivatives showed remarkable effects on anticancer activities. Among them, compound **2c** displayed the most potent inhibitory activity (IC_{50} = 4.8 μM for MCF-7 and IC_{50} = 4.3 μM for Hela), comparable to the positive control ispinesib (IC_{50} = 1.3 μM for MCF-7 and IC_{50} = 1.0 μM for Hela, respectively).

2.3.2. KSP inhibitory activity

The series of flavone and isoflavone derivatives **1a**–**7c** were evaluated for their ability to inhibit the KSP activity and the IC_{50} values of the compounds were summarized in Table 1. It was observed that all the synthesized compounds showed obviously inhibitory activity for KSP with IC_{50} values between 0.023 and 0.170 μM. In particular, compound **2c** had demonstrated the most significant KSP inhibitory activity.

As shown in Table 1, structure–activity relationships in compounds **1a**–**7c** demonstrated that compounds bearing disubstituted nitro-compounds showed better KSP inhibitory activity (**2b**, **2c**, **3a**, **5c**, **6a**–**7c**) than those with monosubstitution (**1a**–**2a**, **3b**, **4a**–**4c**, **5b**). At the same time, perhaps for the same reason, the substitution of chlorine had better activity (**6c**, **7c**), while a loss of activity was observed when it was replaced by a hydrogen atom (**6a**, **7a**). Comparison of the inhibitory activity data also showed that for the compounds possessing the same molecular mass, the IC_{50} value of isoflavone derivatives (**6b**, **6c**) is higher than that observed for flavone derivatives (**2b**, **2c**). Furthermore, influence of the hydroxyl group at C-5 was found to be critical in the determination of the enzyme activity.

The above results indicated that the flavone and isoflavone core along with the NO_2 substitution might have played an important role in the KSP inhibitory activity. Molecular docking of all the compounds of this series had demonstrated the point and this was conformed our estimate.

2.4. Mitotic phenotype

The compounds exhibiting antiproliferating activities in tumor cells and inhibition of KSP *in vitro* were tested for the ability to induce monoastral spindles. Monoastral spindles, the typical phenotype of cells treated with known KSP inhibitors, is formed by the failure of separating the spindle MTs in the nucleation due to loss of KSP activity. The mitotic phenotype of Hela cells and the presence of bipolar and monoastral spindles treated with compound **2c**, **6c** and **4a** were shown in Figs. 3 and 4. The Hela cells treated with compound **2c** at 1 μM gave less obvious phenotype of monoastral spindles compared with that treated at 5 μM. Moreover, at 5 μM, compounds **2c**, **6c** and **4a** were capable of inducing a conspicuous cell morphological change (Fig. 3). And in Fig. 4, we detected that the number of the monoastral spindles appears to increase as the concentration of the compound gets bigger.

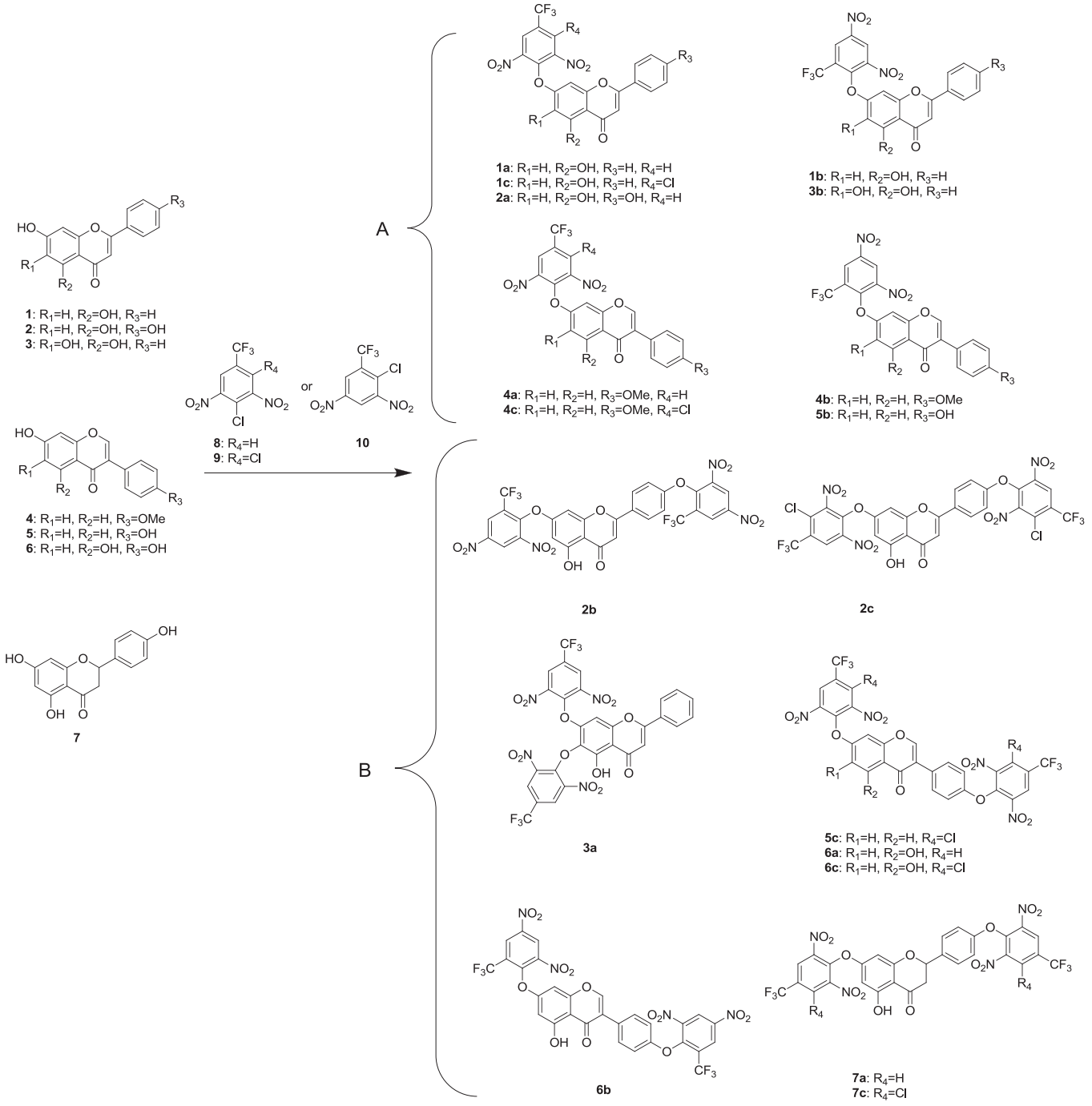

Scheme 1. General synthesis of compounds **1a**–**7c**. Reagents and conditions: (A). 1.0 eq. **8**–**10**, 1.0 eq. t-BuOK, DMF, r t. (B). 2.0 eq. **8**–**10**, 2.0 eq. t-BuOK, DMF, r t.

2.5. Molecular docking study

To gain better understanding on the potency of the synthesized compounds and guide further SAR studies, we proceeded to examine the interaction of the compounds with KSP crystal structure (PDB code: 2Q2Y). The molecular docking was performed by inserting the compounds into the MKR binding site of KSP. All docking runs were applied by Discovery Studio 3.5. The binding model of compound **2c** and KSP was depicted in Fig. 5. The amino acid residues which interacted with KSP were labeled. Docking results revealed that NO_2 group of the compound **2c** played vital roles in the binding pocket, which were stabilized by *Pi-Cation* bond, hydrogen bond, and charge interaction that shown in 2D diagram. Besides, the model suggests that extensive hydrophobic interactions are formed between **2c** and residues Thr112, Pro121, Trp127, Leu132, Ala133, Ile136, Pro137 and Ala218 of the KSP. Most significantly, the interaction between F atom of the compound **2c** and ADP can form a KSP-ADP-**2c** ternary complex, which cannot bind to ATP quickly and subsequently cannot undergo further ATP-driven conformational changes. Overall, these results of the molecular docking, along with the enzyme assay data and mitotic phenotype, suggested that compound **2c** is a potential inhibitor of KSP.

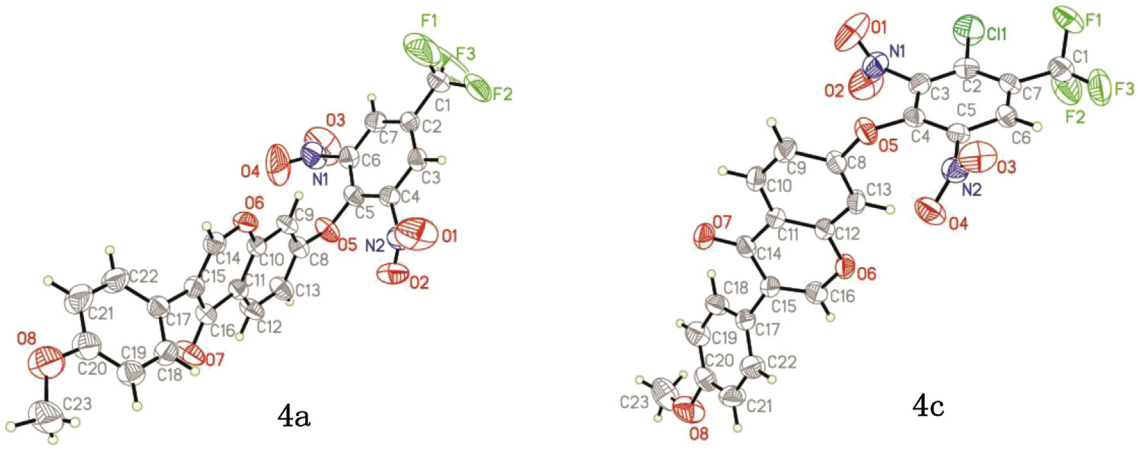

Fig. 2. The molecular structure of compound **4a** and **4c** showing 30% probability displacement ellipsoids for non-hydrogen atoms.

3. Conclusion

In this study, a series of novel KSP inhibitors (**1a**–**7c**) bearing flavone or isoflavone skeleton had been synthesized and evaluated their biological activities. These compounds exhibited potent antiproliferative activities against MCF-7 and Hela cells and KSP inhibitory activities. Among all of the compounds, **2c** showed the most potent inhibition activity which inhibited the growth of MCF-7 and Hela cell lines with IC_{50} values of 4.8 and 4.3 μM and inhibited the KSP with IC_{50} of 0.023 μM. Otherwise, the antiproliferative properties of the synthesized compounds could be explained by their ability to inhibit KSP activity through the mitotic phenotype. Furthermore, after analysis of the docking results, it was found that many interactions between compound **2c** with the protein residues in the binding site might play a crucial role in its KSP inhibitory activities. The information of this work might be helpful for the design and synthesis of KSP inhibitors with stronger activities.

4. Experiments

4.1. Materials and measurements

All chemicals and reagents used in current study were analytical grade. Thin layer chromatography (TLC) was performed on the glass-backed silica gel sheets (Silica Gel 60 GF254) and visualized in UV light (254 nm). Separation of the compounds by column chromatography was carried out with silica gel 60 (200–300 mesh ASTM, E. Merck). The quantity of silica gel used was 50–100 times the weight charged on the column. Melting points were determined on an XT4 MP apparatus (Taike Corp., Beijing, China). All the Proton nuclear magnetic resonance (^{1}H NMR) spectra were recorded on a Bruker PX500 or DPX300 model Spectrometer in DMSO-d_6 at 25 °C with TMS and chemical shifts were reported in parts per million (d). The solvent signals allotted as internal stands. Elemental analyses were performed on a CHN–O-Rapid instrument. All the compounds gave satisfactory chemical analyses (±0.4%).

Table 1
Antiproliferative and inhibitory activities of compounds **1a**–**7c** (IC_{50}, μM).

Compounds	MCF-7	Hela	KSP
1a	14.9 ± 1.24	13.9 ± 1.37	0.134 ± 0.024
1b	15.6 ± 1.38	14.8 ± 1.36	0.122 ± 0.013
1c	12.7 ± 1.09	14.2 ± 1.51	0.123 ± 0.032
2a	13.2 ± 1.20	12.8 ± 1.27	0.098 ± 0.010
2b	5.2 ± 0.48	4.9 ± 0.44	0.027 ± 0.0018
2c	4.8 ± 0.45	4.3 ± 0.39	0.023 ± 0.0014
3a	5.1 ± 0.56	5.3 ± 0.52	0.038 ± 0.0030
3b	12.9 ± 1.33	15.3 ± 1.39	0.091 ± 0.0087
4a	13.6 ± 1.42	17.8 ± 1.65	0.168 ± 0.034
4b	19.8 ± 1.76	17.6 ± 1.37	0.170 ± 0.031
4c	15.4 ± 1.20	18.9 ± 1.82	0.157 ± 0.037
5b	15.7 ± 1.34	16.9 ± 1.26	0.149 ± 0.029
5c	12.6 ± 1.32	11.2 ± 1.17	0.076 ± 0.0043
6a	9.9 ± 0.90	10.2 ± 1.20	0.067 ± 0.0035
6b	11.3 ± 1.09	10.8 ± 1.06	0.078 ± 0.0058
6c	9.8 ± 0.86	9.6 ± 0.80	0.063 ± 0.0046
7a	8.9 ± 0.75	9.0 ± 0.92	0.059 ± 0.0039
7c	8.2 ± 0.72	7.8 ± 0.67	0.052 ± 0.0050
Ispinesib	1.3 ± 0.10	1.0 ± 0.08	0.005 ± 0.0002

4.2. General procedure for the synthesis of flavone and isoflavone derivatives (*1a*–*7c*)

The synthesis of flavone and isoflavone derivatives followed the general reaction pathway outlined in Scheme 1. The substituted dinitro-compounds (series A: 1 mmol; series B: 2 mmol) mixed with flavones or isoflavones (1 mmol) through by using t-BuOK (series A: 1 mmol; series B: 2 mmol) as catalyst in 20–30 ml DMF for 3–4 h at room temperature. The reaction was monitored by TLC.

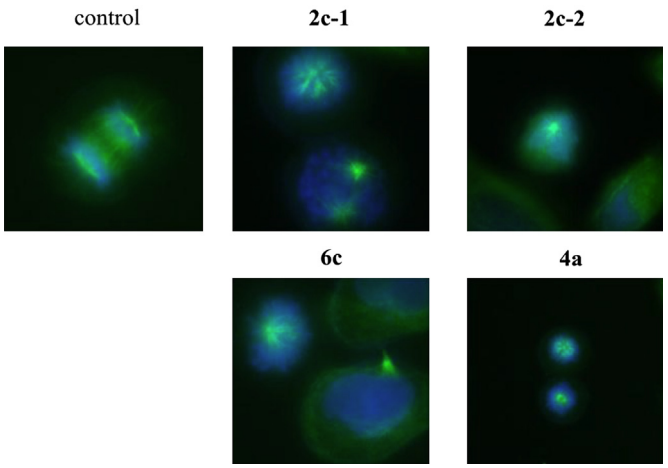

Fig. 3. Mitotic phenotype of Hela cells with flavone and isoflavone derivatives **2c-1** (**2c**: 1 μM), **2c-2** (**2c**: 5 μM), **6c** (5 μM) and **4a** (5 μM). Microtubules are colored in green, and DNA in blue. (For interpretation of the references to color in this figure legend, the reader is referred to the web version of this article.)

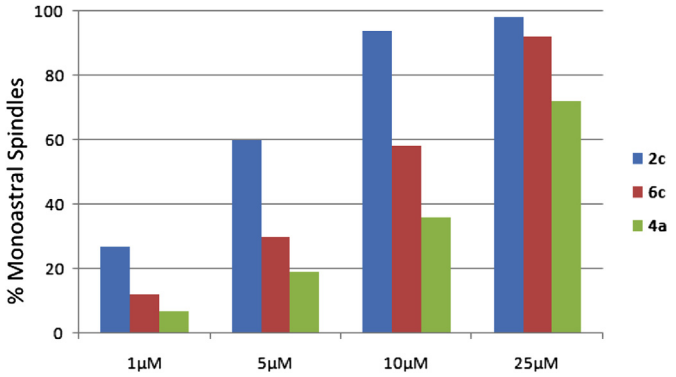

Fig. 4. The presence of bipolar spindles and monoastral spindles were scored in four different concentrations of each of the indicated inhibitors in Hela cells, and the % of monoastral spindles were determined and plotted as bar graphs.

The products are extracted with ethyl acetate and saturated salt water, dried over Na_2SO_4, filtered and evaporated. The residue is purified by column chromatography using petroleum ether and ethyl acetate.

*4.2.1. 7-(2,6-Dinitro-4-(trifluoromethyl)phenoxy)-5-hydroxy-2-phenyl-4H-chromen-4-one (**1a**)*

White powder, yield: 80%. Mp: 176–178 °C. ^{1}H NMR (500 MHz, $CDCl_3$, δ ppm): 6.26 (d, J = 2.10 Hz, 1H); 6.56 (d, J = 2.15 Hz, 1H); 6.73 (s, 1H); 7.51–7.57 (m, 3H); 7.87 (d, J = 7.45 Hz, 2H); 8.55 (s, 2H); 12.90 (s, 1H). MS (ESI): 489.1 ([M + H]$^+$). Anal. Calcd for $C_{22}H_{11}F_3N_2O_8$: C, 54.11; H, 2.27; N, 5.74%; Found: C, 54.23; H, 2.19; N, 5.64%.

*4.2.2. 7-(2,4-Dinitro-6-(trifluoromethyl)phenoxy)-5-hydroxy-2-phenyl-4H-chromen-4-one (**1b**)*

White powder, yield: 75%. Mp: 158–160 °C. ^{1}H NMR (500 MHz, $CDCl_3$, δ ppm): 5.93 (s, 1H); 6.24 (d, J = 2.15 Hz, 1H); 6.51 (d, J = 2.15 Hz, 1H); 7.50–7.58 (m, 3H); 7.86 (d, J = 7.30 Hz, 2H); 8.91 (d, J = 2.50 Hz, 1H); 9.13 (d, J = 2.55 Hz, 1H). MS (ESI): 489.1 ([M + H]$^+$). Anal. Calcd for $C_{22}H_{11}F_3N_2O_8$: C, 54.11; H, 2.27; N, 5.74%; Found: C, 54.02; H, 2.18; N, 5.68%.

*4.2.3. 7-(3-Chloro-2,6-dinitro-4-(trifluoromethyl)phenoxy)-5-hydroxy-2-phenyl-4H-chromen-4-one (**1c**)*

Yellow powder, yield: 82%. Mp: 232–234 °C. ^{1}H NMR (300 MHz, $CDCl_3$, δ ppm): 6.32 (d, J = 2.34 Hz, 1H); 6.57 (d, J = 2.37 Hz, 1H); 6.74 (s, 1H); 7.54–7.59 (m, 3H); 7.87–7.90 (m, 2H); 8.64 (s, 1H); 12.92 (s, 1H). MS (ESI): 523.8 ([M + H]$^+$). Anal. Calcd for $C_{22}H_{10}ClF_3N_2O_8$: C, 50.55; H, 1.93; N, 5.36%; Found: C, 50.67; H, 1.87; N, 5.25%.

*4.2.4. 7-(2,6-Dinitro-4-(trifluoromethyl)phenoxy)-5-hydroxy-2-(4-hydroxyphenyl)-4H-chromen-4-one (**2a**)*

Yellow powder, yield: 84%. Mp: 258–260 °C. ^{1}H NMR (300 MHz, DMSO-d_6, δ ppm): 6.64 (d, J = 2.34 Hz, 1H); 7.01–7.12 (m, 2H); 8.10 (d, J = 8.82 Hz, 2H); 8.97 (d, J = 8.13 Hz, 4H); 12.98 (s, 1H). MS (ESI): 505.3 ([M + H]$^+$). Anal. Calcd for $C_{22}H_{11}F_3N_2O_9$: C, 52.39; H, 2.20; N, 5.55%; Found: C, 52.21; H, 2.18; N, 5.63%.

*4.2.5. 7-(2,4-Dinitro-6-(trifluoromethyl)phenoxy)-2-(4-(2,4-dinitro-6-(trifluoromethyl)phenoxy)phenyl)-5-hydroxy-4H-chromen-4-one (**2b**)*

Yellow powder, yield: 76%. Mp: 237 °C. ^{1}H NMR (300 MHz, $CDCl_3$, δ ppm): 6.23 (d, J = 2.28 Hz, 1H); 6.52 (d, J = 2.31 Hz, 1H); 6.67 (s, 1H); 7.01 (d, J = 8.79 Hz, 2H); 7.87 (d, J = 8.82 Hz, 2H); 8.92 (d, J = 2.49 Hz, 2H); 9.11 (dd, J_1 = 2.67 Hz, J_2 = 17.34 Hz, 2H); 12.82 (s, 1H). MS (ESI): 739.0 ([M + H]$^+$). Anal. Calcd for $C_{29}H_{12}F_6N_4O_{13}$: C, 47.17; H, 1.64; N, 7.59%; Found: C, 47.22; H, 1.58; N, 7.67%.

*4.2.6. 7-(3-Chloro-2,6-dinitro-4-(trifluoromethyl)phenoxy)-2-(4-(3-chloro-2,6-dinitro-4-(trifluoromethyl)phenoxy)phenyl)-5-hydroxy-4H-chromen-4-one (**2c**)*

Yellow powder, yield: 78%. Mp: 253–255 °C. ^{1}H NMR (300 MHz, DMSO-d_6, δ ppm): 6.74 (d, J = 2.40 Hz, 1H); 7.11–7.16 (m, 2H); 7.39 (d, J = 9.03 Hz, 2H); 8.11 (d, J = 9.03 Hz, 2H); 8.87 (d, J = 7.26 Hz, 2H); 12.99 (s, 1H). MS (ESI): 807.0 ([M + H]$^+$). Anal. Calcd for $C_{29}H_{10}Cl_2F_6N_4O_{13}$: C, 43.14; H, 1.25; N, 6.94%; Found: C, 43.26; H, 1.34; N, 6.85%.

*4.2.7. 6,7-Bis(2,6-dinitro-4-(trifluoromethyl)phenoxy)-5-hydroxy-2-phenyl-4H-chromen-4-one (**3a**)*

Yellow powder, yield: 78%. Mp: 189–190 °C. ^{1}H NMR (300 MHz, $CDCl_3$, δ ppm): 6.55–6.74 (m, 3H); 7.46–7.49 (m,4H); 7.78–7.81 (m, 2H); 8.31–8.52 (m, 2H); 13.02 (m, 1H). MS (ESI): 739.0 ([M + H]$^+$).

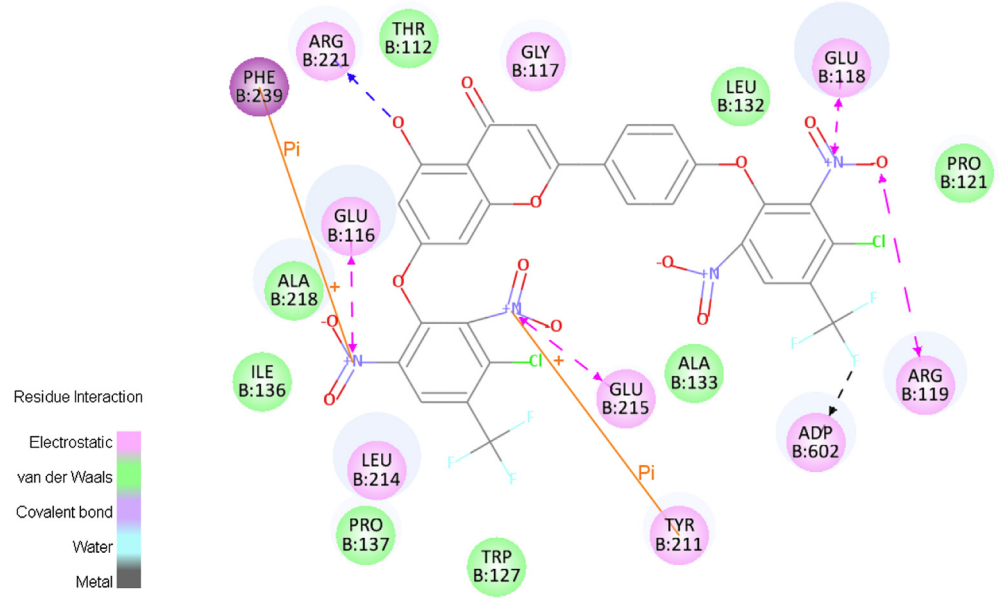

Fig. 5. 2D diagram of binding model between KSP and compound **2c**.

Anal. Calcd for $C_{29}H_{12}F_6N_4O_{13}$: C, 47.17; H, 1.64; N, 7.59%; Found: C, 47.23; H, 1.58; N, 7.72%.

4.2.8. 7-(2,4-Dinitro-6-(trifluoromethyl)phenoxy)-5,6-dihydroxy-2-phenyl-4H-chromen-4-one (**3b**)

Yellow powder, yield: 83%. Mp: 236–238 °C. ^{1}H NMR (300 MHz, DMSO-d_6, δ ppm): 6.68 (s, 1H); 7.03 (s, 1H); 7.58–7.64 (m, 3H); 8.08–8.11 (m, 2H); 8.75 (d, J = 2.67 Hz, 1H); 9.03 (d, J = 2.67 Hz, 1H); 11.79 (s, 1H); 13.26 (s, 1H). MS (ESI): 505.0 ([M + H]$^+$). Anal. Calcd for $C_{22}H_{11}F_3N_2O_9$: C, 52.39; H, 2.20; N, 5.55%; Found: C, 52.46; H, 2.13; N, 5.72%.

4.2.9. 7-(2,6-Dinitro-4-(trifluoromethyl)phenoxy)-3-(4-methoxyphenyl)-4H-chromen-4-one (**4a**)

White powder, yield: 85%. Mp: 188–190 °C. ^{1}H NMR (500 MHz, $CDCl_3$, δ ppm): 3.84 (s, 3H); 6.93–6.98 (m, 4H); 7.48 (d, J = 8.55 Hz, 2H); 7.93 (s, 1H); 8.32 (d, J = 8.70 Hz, 1H); 8.54 (s, 2H). MS (ESI): 503.1 ([M + H]$^+$). Anal. Calcd for $C_{23}H_{13}F_3N_2O_8$: C, 54.99; H, 2.61; N, 5.58%; Found: C, 54.70; H, 2.68; N, 5.66%.

4.2.10. 7-(2,4-Dinitro-6-(trifluoromethyl)phenoxy)-3-(4-methoxyphenyl)-4H-chromen-4-one (**4b**)

White powder, yield: 83%. Mp: 184–186 °C. ^{1}H NMR (500 MHz, $CDCl_3$, δ ppm): 3.84 (s, 3H); 6.88–6.98 (m, 4H); 7.47–7.49 (m, 2H); 7.93 (s, 1H); 8.31 (d, J = 3.80 Hz, 1H); 8.92 (d, J = 2.50 Hz, 1H); 9.11 (d, J = 2.70 Hz, 1H). MS (ESI): 503.1 ([M + H]$^+$). Anal. Calcd for $C_{23}H_{13}F_3N_2O_8$: C, 54.99; H, 2.61; N, 5.58%; Found: C, 54.77; H, 2.63; N, 5.69%.

4.2.11. 7-(3-Chloro-2,6-dinitro-4-(trifluoromethyl)phenoxy)-3-(4-methoxyphenyl)-4H-chromen-4-one (**4c**)

White powder, yield: 78%. Mp: 168–170 °C. ^{1}H NMR (500 MHz, $CDCl_3$, δ ppm): 3.77 (s, 3H); 6.90–6.94 (m, 4H); 7.41 (d, J = 8.65 Hz, 2H); 7.87 (s, 1H); 8.25 (d, J = 8.85 Hz, 1H); 8.55 (s, 1H). MS (ESI): 537.0 ([M + H]$^+$). Anal. Calcd for $C_{23}H_{12}ClF_3N_2O_8$: C, 51.46; H, 2.25; N, 5.22%; Found: C, 51.35; H, 2.22; N, 5.29%.

4.2.12. 7-(2,4-Dinitro-6-(trifluoromethyl)phenoxy)-3-(4-hydroxyphenyl)-4H-chromen-4-one (**5b**)

White powder, yield: 76%. Mp: 192–194 °C. ^{1}H NMR (500 MHz, $CDCl_3$, δ ppm): 6.79 (s, 1H); 6.86 (d, J = 2.80 Hz, 3H); 7.50 (d, J = 8.60 Hz, 2H); 7.96–7.98 (m, 2H); 8.80 (d, J = 2.15 Hz, 1H); 9.02 (d, J = 2.35 Hz, 1H). MS (ESI): 489.1 ([M + H]$^+$). Anal. Calcd for $C_{22}H_{11}F_3N_2O_8$: C, 54.11; H, 2.27; N, 5.74%; Found: C, 54.32; H, 2.36; N, 5.68%.

4.2.13. 7-(3-Chloro-2,6-dinitro-4-(trifluoromethyl)phenoxy)-3-(4-(3-chloro-2,6-dinitro-4-(trifluoromethyl)phenoxy)phenyl)-4H-chromen-4-one (**5c**)

Yellow powder, yield: 77%. Mp: 251–253 °C. ^{1}H NMR (300 MHz, $CDCl_3$, δ ppm): 6.99–7.02 (m, 4H); 7.56 (d, J = 8.64 Hz, 2H); 7.98 (s, 1H); 8.32 (d, J = 8.70 Hz, 1H); 8.54 (s, 1H); 8.64 (s, 1H). MS (ESI): 791.0 ([M + H]$^+$). Anal. Calcd for $C_{29}H_{10}Cl_2F_6N_4O_{12}$: C, 44.02; H, 1.27; N, 7.08%; Found: C, 44.32; H, 1.35; N, 7.26%.

4.2.14. 7-(2,6-Dinitro-4-(trifluoromethyl)phenoxy)-3-(4-(2,6-dinitro-4-(trifluoromethyl)phenoxy)phenyl)-5-hydroxy-4H-chromen-4-one (**6a**)

White powder, yield: 83%. Mp: 221–222 °C. ^{1}H NMR (300 MHz, DMSO-d_6, δ ppm): 6.67 (d, J = 2.40 Hz, 1H); 6.96 (d, J = 2.40 Hz, 1H); 7.16 (dd, J_1 = 2.07 Hz, J_2 = 6.84 Hz, 2H); 7.55–7.58 (m, 2H); 8.59 (s, 1H); 8.95 (d, J = 8.10 Hz, 4H); 12.97 (s, 1H). MS (ESI): 739.0 ([M + H]$^+$). Anal. Calcd for $C_{29}H_{12}F_6N_4O_{13}$: C, 47.17; H, 1.64; N, 7.59%; Found: C, 47.28; H, 1.54; N, 7.72%.

4.2.15. 7-(2,4-Dinitro-6-(trifluoromethyl)phenoxy)-3-(4-(2,4-dinitro-6-(trifluoromethyl)phenoxy)phenyl)-5-hydroxy-4H-chromen-4-one (**6b**)

Yellow powder, yield: 75%. Mp: 212–213 °C. ^{1}H NMR (300 MHz, DMSO-d_6, δ ppm): 6.61 (d, J = 2.34 Hz, 1H); 6.90 (d, J = 2.34 Hz, 1H); 7.11 (d, J = 8.82 Hz, 2H); 7.57 (d, J = 8.88 Hz, 2H); 8.58 (s, 1H); 8.92 (dd, J_1 = 2.67 Hz, J_2 = 7.11 Hz, 2H); 9.22 (dd, J_1 = 2.70 Hz, J_2 = 10.71 Hz, 2H); 12.95 (s, 1H). MS (ESI): 739.0 ([M + H]$^+$). Anal. Calcd for $C_{29}H_{12}F_6N_4O_{13}$: C, 47.17; H, 1.64; N, 7.59%; Found: C, 47.32; H, 1.60; N, 7.68%.

4.2.16. 7-(3-Chloro-2,6-dinitro-4-(trifluoromethyl)phenoxy)-3-(4-(3-chloro-2,6-dinitro-4-(trifluoromethyl)phenoxy)phenyl)-5-hydroxy-4H-chromen-4-one (**6c**)

Yellow powder, yield: 73%. Mp: 236–238 °C. ^{1}H NMR (300 MHz, DMSO-d_6, δ ppm): 6.32 (d, J = 2.40 Hz, 1H); 6.51 (d, J = 2.37 Hz, 1H); 7.02 (d, J = 8.82 Hz, 2H); 7.53 (d, J = 8.82 Hz, 2H); 7.96 (s, 1H); 8.49–8.64 (m, 2H); 12.85 (s, 1H). MS (ESI): 807.0 ([M + H]$^+$). Anal. Calcd for $C_{29}H_{10}Cl_2F_6N_4O_{13}$: C, 43.14; H, 1.25; N, 6.94%; Found: C, 43.26; H, 1.31; N, 6.87%.

4.2.17. 7-(2,6-Dinitro-4-(trifluoromethyl)phenoxy)-2-(4-(2,6-dinitro-4-(trifluoromethyl)phenoxy)phenyl)-5-hydroxychroman-4-one (**7a**)

Yellow powder, yield: 85%. Mp: 160–162 °C. ^{1}H NMR (300 MHz, $CDCl_3$, δ ppm): 2.87 (dd, J_1 = 3.00 Hz, J_2 = 17.22 Hz, 1H); 3.12 (dd, J_1 = 13.38 Hz, J_2 = 17.22 Hz, 1H); 5.45 (dd, J_1 = 2.88 Hz, J_2 = 13.38 Hz, 1H); 6.04 (dd, J_1 = 2.40 Hz, J_2 = 5.76 Hz, 2H); 6.97 (d, J = 8.73 Hz, 2H); 7.43 (d, J = 8.76 Hz, 2H); 8.47 (s, 2H); 8.53 (s, 2H); 11.97 (s, 1H). MS (ESI): 741.1 ([M + H]$^+$). Anal. Calcd for $C_{29}H_{14}F_6N_4O_{13}$: C, 47.04; H, 1.91; N, 7.57%; Found: C, 47.15; H, 1.87; N, 7.62%.

4.2.18. 7-(3-Chloro-2,6-dinitro-4-(trifluoromethyl)phenoxy)-2-(4-(3-chloro-2,6-dinitro-4-(trifluoromethyl)phenoxy)phenyl)-5-hydroxychroman-4-one (**7c**)

Yellow powder, yield: 72%. Mp: 213–214 °C. ^{1}H NMR (300 MHz, $CDCl_3$, δ ppm): 2.84 (d, J = 3.03 Hz, 1H); 3.11 (dd, J_1 = 13.32 Hz, J_2 = 17.25 Hz, 1H); 5.43–5.48 (m, 1H); 6.06 (dd, J_1 = 2.43 Hz, J_2 = 13.11 Hz, 2H); 7.00 (d, J = 8.76 Hz, 2H); 7.43 (d, J = 8.70 Hz, 2H); 8.58 (d, J = 23.22 Hz, 2H); 11.95 (s, 1H). MS (ESI): 809.0 ([M + H]$^+$). Anal. Calcd for $C_{29}H_{12}Cl_2F_6N_4O_{13}$: C, 43.04; H, 1.49; N, 6.92%; Found: C, 43.13; H, 1.52; N, 6.87%.

4.3. Crystal structure determination

Crystal structure determination of compound **4a** and **4c** were carried out on a Nonius CAD4 diffractometer equipped with graphitemonochromated Mo*Ka* (k = 0.71073 Å) radiation. The structure was solved by direct methods and refined on F^2 by full-matrix least-squares methods using SHELX-97. All non-hydrogen atoms of compound **4a** and **4c** were refined with anisotropic thermal parameters. All hydrogen atoms were placed in geometrically idealized positions and constrained to ride on their parent atoms.

4.4. Antiproliferation activity

The antiproliferative activities of the prepared compounds against MCF-7 and Hela cell lines were evaluated as described elsewhere with some modifications [24]. Target tumor cell lines were grown to log phase in RPMI 1640 medium supplemented with 10% fetal bovine serum. After diluting to 2×10^4 cells/mL with the complete medium, 100 μL of the obtained cell suspension was added to each well of 96-well culture plates. The subsequent incubation was permitted at 37 °C, 5% CO_2 atmosphere for 24 h before the cytotoxicity assessments. Tested samples at pre-set concentrations

were added to six wells with ispinesib as positive references. After 48 h exposure period, 40 μL of PBS containing 2.5 mg/mL of MTT (3-(4,5-dimethylthiazol-2-yl)-2,5-diphenyltet-razolium bromide) was added to each well. Four hours later, 100 μL extraction solution (10% SDS-5% isobutyl alcohol −0.01 M HCl) was added. After an overnight incubation at 37 °C, the optical density was measured at a wavelength of 570 nm on an ELISA microplate reader. In all experiments, three replicate wells were used for each drug concentration. Each assay was carried out for at least three times.

4.5. KSP inhibitory assay

The microtubule-stimulated KSP ATPase reaction was performed in a reaction buffer [20 mM PIPES-K (pH 6.8), 25 mM KCl, 2 mM $MgCl_2$, 1 mM EGTA-KOH (pH 8.0)] containing 38 nM bacteria-expressed KSP motor domain (1–369) fused to a histidine tag at the carboxyl terminus and 350 nM microtubules in 96-well half-area plates (Corning). Each chemical compound in DMSO at different concentrations was diluted 12.5-fold with the chemical dilution buffer [10 mM Tris-OAc (pH 7.4), 0.04% (v/v) NP-40]. After pre-incubation of 9.7 μL of the enzyme solution with 3.8 μL of each chemical solution at 25 °C for 30 min, the ATPase reaction was initiated by the addition of 1.5 μL of 0.3 mM ATP, followed by incubation at 25 °C for 15 min. The reaction was terminated by the addition of 15 μL Kinase-Glo Plus reagent (Promega). The ATP consumption in each reaction was measured as the luciferase-derived luminescence by ARVO Light (PerkinElmer). At least three experiments were performed per condition, and the averages and standard deviations of inhibition rates in each condition were evaluated to determine IC_{50} values using Microsoft Excel and GraphPad Prism software [25].

4.6. Immunofluorescence microscopy

HeLa cells were grown in DMEM (Gibco BRL; Paisley, UK), supplemented with 10% fetal calf serum (Hyclone) on poly-D-lysine (Sigma–Aldrich)-coated 12-mm diameter glass coverslips in 24-well plates. Cells were seeded and allowed to adhere for at least 36 h before drug addition. Drugs were diluted appropriately in medium from 25 mM stocks in 100% DMSO and then added to the cells. Following 8 h incubation with drugs, cells were fixed by incubation in 2% paraformaldehyde (20 min at 37 °C) and permeabilized with 0.2% Triton X-100 in PBS for 3 min before being incubated with primary and stained with secondary antibodies. Cells were stained with anti-β-tubulin monoclonal antibodies (Sigma) at 400-fold dilution for 1 h and then with Alexa fluor 488-conjugated goat antimouse secondary antibodies (Invitrogen) at 300-fold dilution for 30 min; DNA was detected with 4′, 6-diamidino-2-phenylindole dihydrochloride (DAPI) with VECTASHIELD mounting medium. The percentage of mitotic cells with monoastral spindles present in treated cells was calculated over the total number of cells in mitosis counted after 8 h incubation with drugs. Images were collected with an inverted Olympus IX81 epifluorescence motorized microscope equipped with a motorized piezo stage (Ludl Electronic Products, Hawthorne, NY) and a Retiga-SRV CCD camera (QImaging) driven by VOLOCITY software (Improvision) with a binning of 1, using a PlanApo 60 × NA1.42 objective (Olympus). Images were processed in Photoshop version 7.0 (Adobe) and assembled in CANVAS version 8.0 (Denaba Systems) [25].

4.7. Docking simulations

The three-dimensional X-ray structure of KSP (PDB code: 2Q2Y) was chosen as the template for the modeling study of the synthesized compounds. The pdb file about the crystal structure of the KSP domain bound to MKR (2Q2Y.pdb) was obtained from the RCSB protein data bank (http://www.pdb.org). The molecular docking procedure was performed by using CDOCKER protocol for receptor–ligand interactions section of Discovery Studio 3.5 (Accelrys Software Inc, San Diego, CA) [26]. All bound water and ligands were eliminated from the protein and the polar hydrogen was added. The whole KSP complex was defined as a receptor and the site sphere was selected based on the ligand binding location of MKR, then the MKR molecule was removed and the tested compound was placed during the molecular docking procedure. Types of interactions of the docked protein with ligand were analyzed after the end of molecular docking.

Acknowledgments

This work was supported by Major Projects on Control and Rectification of Water Body Pollution (No. 2011ZX07204-001-004), and was supported by 'PCSIRT' (IRT1020).

Appendix A. Supplementary data

Supplementary data related to this article can be found at http://dx.doi.org/10.1016/j.ejmech.2013.09.042.

References

[1] M.A. Jordan, L. Wilson, Nat. Rev. Cancer 4 (2004) 253–265.
[2] F.E. Samson, J. Neurobiol. 2 (1971) 347–360.
[3] S.Y. Chan, R. Worth, S. Ochs, J. Neurobiol. 11 (1980) 251–264.
[4] L.C. Kapitein, E.J. Peterman, B.H. Kwok, J.H. Kim, T.M. Kapoor, C.F. Schmidt, Nature 435 (2005) 114–118.
[5] A. Slangy, H.A. Lane, P. D'Hérin, M. Harper, M. Kress, E.A. Niggt, Cell 83 (1995) 1159–1169.
[6] T.U. Mayer, T.M. Kapoor, S.J. Haggarty, R.W. King, S.L. Schreiber, T.J. Mitchison, Science 286 (1999) 971–974.
[7] R. Sakowicz, J.T. Finer, C. Beraud, A. Crompton, E. Lewis, A. Fritsch, Y. Lee, J. Mak, R. Moody, R. Turincio, Cancer Res. 64 (2004) 3276–3280.
[8] G.M. Hansen, M.J. Justice, Oncogene 18 (1999) 6531.
[9] P.S. Hegde, J. Cogswell, K. Carrick, J. Jackson, K.W. Wood, W.K. Eng, M. Brawner, P.S. Huang, D. Bergsma, Proc. Am. Soc. Clin. Oncol. 22 (2003) 535.
[10] B.Z. Carter, D.H. Mak, Y. Shi, W.D. Schober, R. Wang, M. Konopleva, E. Koller, N.M. Dean, M. Andreeff, Cell Cycle 5 (2006) 2223–2229.
[11] C.D. Cox, P.J. Coleman, M.J. Breslin, D.B. Whitman, R.M. Garbaccio, M.E. Fraley, C.A. Buser, E.S. Walsh, K. Hamilton, M.D. Schaber, J. Med. Chem. 51 (2008) 4239–4252.
[12] B.Z. Carter, D.H. Mak, R. Woessner, S. Gross, W.D. Schober, Z. Estrov, H. Kantarjian, M. Andreeff, Leukemia 23 (2009) 1755–1762.
[13] M.E. Fraley, R.M. Garbaccio, K.L. Arrington, W.F. Hoffman, E.S. Tasber, P.J. Coleman, C.A. Buser, E.S. Walsh, K. Hamilton, C. Fernandes, Bioorg. Med. Chem. Lett. 16 (2006) 1775–1779.
[14] R.M. Garbaccio, M.E. Fraley, E.S. Tasber, C.M. Olson, W.F. Hoffman, K.L. Arrington, M. Torrent, C.A. Buser, E.S. Walsh, K. Hamilton, Bioorg. Med. Chem. Lett. 16 (2006) 1780–1783.
[15] A.J. Roecker, P.J. Coleman, S.P. Mercer, J.D. Schreier, C.A. Buser, E.S. Walsh, K. Hamilton, R.B. Lobell, W. Tao, R.E. Diehl, Bioorg. Med. Chem. Lett. 17 (2007) 5677–5682.
[16] Y. Yan, V. Sardana, B. Xu, C. Homnick, W. Halczenko, C.A. Buser, M. Schaber, G.D. Hartman, H.E. Huber, L.C. Kuo, J. Mol. Biol. 335 (2004) 547–554.
[17] J.R. Jackson, D.R. Patrick, M.M. Dar, P.S. Huang, Nat. Rev. Cancer 7 (2007) 107–117.
[18] G.W. Mayr, S. Windhorst, K. Hillemeier, J. Biol. Chem. 280 (2005) 13229–13240.
[19] B.K. Chacko, R.T. Chandler, A. Mundhekar, N. Khoo, H.M. Pruitt, D.F. Kucik, D.A. Parks, C.G. Kevil, S. Barnes, R.P. Patel, Am. J. Physiol.-Heart C 289 (2005) H908–H915.
[20] X. Wang, E.A. Clubbs, J.A. Bomser, J. Nutr. Biochem. 17 (2006) 204–210.
[21] I.R. Record, I.E. Dreosti, J.K. McInerney, J. Nutr. Biochem. 6 (1995) 481–485.
[22] J.N. Davis, O. Kucuk, F.H. Sarkar, Nutr. Cancer 35 (1999) 167–174.
[23] G. Zinzalla, D.E. Thurston, 2009.
[24] A. Boumendjel, J. Boccard, P. Carrupt, E. Nicolle, M. Blanc, A. Geze, L. Choisnard, D. Wouessidjewe, E. Matera, C. Dumontet, J. Med. Chem. 51 (2008) 2307–2310.
[25] S. Nagarajan, D.A. Skoufias, F. Kozielski, A.N. Pae, J. Med. Chem. 55 (2012) 2561–2573.
[26] G. Wu, D.H. Robertson, C.L. Brooks, M. Vieth, J. Comput. Chem. 24 (2003) 1549–1562.